Osmotic pressure effects identify dehydration upon cytochrome *c* - cytochrome *c* oxidase complex formation contributing to a specific electron pathway formation

Wataru Sato[1], *Seiji Hitaoka*[2], *Takeshi Uchida*[1,3], *Kyoko Shinzawa-Itoh*[4], *Kazunari Yoshizawa*[2], *Shinya Yoshikawa*[4], *and Koichiro Ishimori*[1,3,*]

[1]Graduate School of Chemical Sciences and Engineering, Hokkaido University, Sapporo 060-8628, Japan,

[2]Institute for Materials Chemistry and Engineering, Kyushu University, Fukuoka 819-0315, Japan,

[3]Department of Chemistry, Faculty of Science, Hokkaido University, Sapporo 060-0810, Japan,

[4]Picobiology Institute, Graduate School of Life Science, University of Hyogo, Ako-gun, Hyogo 678-1297, Japan.

*Corresponding Author

E-mail: koichiro@sci.hokudai.ac.jp (K.I.). Phone: 81(11) 706-2707

Key Words

Cytochrome *c*, Cytochrome *c* Oxidase, Osmotic Pressure, Electron Transfer, Dehydration

ABSTRACT

In the electron transfer (ET) reaction from cytochrome *c* (Cyt *c*) to cytochrome *c* oxidase (C*c*O), we determined the number and sites of the hydration water released from the protein surface upon formation of the ET complex by evaluating the osmotic pressure dependence of kinetics for the ET from Cyt *c* to C*c*O. We identified that approximately 20 water molecules were dehydrated in complex formation under turnover conditions, and systematic Cyt *c* mutations in the interaction site for C*c*O revealed that nearly half of the released hydration water during the complexation were located around Ile81, one of the hydrophobic amino acid residues near the exposed heme periphery of Cyt *c*. Such a dehydration dominantly compensates for the entropy decrease due to the association of Cyt *c* with C*c*O, resulting in the entropy-driven ET reaction. The energetic analysis of the interprotein interactions in the ET complex predicted by the docking simulation suggested the formation of hydrophobic interaction sites surrounding the exposed heme periphery of Cyt *c* in the Cyt *c* – C*c*O interface (a "molecular breakwater"). Such sites would contribute to formation of the hydrophobic ET pathway from Cyt *c* to C*c*O by blocking water access from the bulk water phase.

INTRODUCTION

Electron transfer (ET) in the respiratory chain is the most essential process of energy transduction in cells[1]. Driven by ET, protons are pumped from the negative space to positive space in mitochondria, resulting in a proton concentration gradient across the inner mitochondrial membrane. The electrochemical potential induced by the process is the driving force for ATP synthesis by membrane-bound ATPase.

The final ET in the respiratory chain is mediated by a small hemoprotein, cytochrome *c* (Cyt *c*)[2], which carries one electron from the cytochrome bc_1 complex (Complex III) to cytochrome *c* oxidase (C*c*O, Complex IV). Through the electron flow from Complex III, C*c*O can reduce molecular oxygen to water molecules to terminate the respiratory chain, where four electrons are used to reduce one molecule of dioxygen, in conjunction with proton pumping. Cyt *c* is a one-electron carrier, and the repetitive binding of Cyt *c* is required to reduce molecular oxygen. Because efficiency of the proton pump coupled with the dioxygen reduction in C*c*O depends on the ET reaction from Cyt *c* to C*c*O[3], specific interactions between Cyt *c* and C*c*O are essential for energy transduction in the respiratory chain.

We have determined the interaction site for C*c*O on Cyt *c* by NMR[4] and revealed that certain hydrophobic amino acid residues are located in the interaction site, along with previously reported positively charged residues[5, 6]. Our energetic analysis of the simulated Cyt *c* – C*c*O complex also indicates the primary contribution of hydrophobic interactions to the stability of the Cyt *c* – C*c*O complex[7]. A recent X-ray study of the Cyt *c* – C*c*O complex also showed that some hydrophobic amino acid residues are located in the interface, but there are no intermolecular interactions between hydrophobic amino acid residues with an interatomic distance < 5 Å[8].

Although both NMR and X-ray studies suggest critical involvements of hydrophobic residues on complex formation, it has not yet been shown experimentally how these hydrophobic residues (or hydrophobic interactions) contribute to the stability of the ET complex and the ET reaction. The detailed stabilization mechanism for complex formation by hydrophobic interactions and functional significance of the formation of the hydrophobic interactions are, therefore, still key open questions in the ET reaction from Cyt *c* to C*c*O.

One line of experimental evidence shows that the hydrophobic interactions that occur in protein-protein complexes involve the dehydration of the hydrophobic amino acid residues in the interaction site[9, 10]. The hydrophobic side chains of amino acid residues on the protein surface, as well as the side chains of hydrophilic amino acid residues, are hydrated. If hydrophobic amino acid residues are part of the interaction site with the partner protein, the hydrating water molecules would be expelled from the protein surface to allow the amino acid residues to form hydrophobic interactions with the amino acid residues of the partner proteins. Such dehydration is observed for both hydrophobic and hydrophilic amino acid residues[11, 12], but the energetic contribution of hydrophobic interactions to the formation of the protein-protein complex is much larger than the contribution of hydrophilic interactions[13], thus suggesting that the dehydration of hydrophobic amino acid residues is a key process in the formation of the Cyt *c* – C*c*O complex that facilitates the ET reaction.

Here, we focused on the change in the partial molar volume of proteins[14], which is altered during dehydration associated with the formation of the Cyt *c* – C*c*O complex. Assuming that the molecular volume of each protein is unchanged after complex formation, the change in the partial molecular volume corresponds to the volume of the water molecules involved in dehydration (negative volume change) or hydration (positive volume change)[15, 16]. The volume

changes during the formation of the protein-protein complex might be estimated from a precise measurement of the difference in the volumes before and after complex formation, but the heat of the reaction and the mixing of the solution complicate interpretation of the results[17]. However, the partial molar volume change associated with complex formation is simply correlated with the osmotic pressure dependence of the dissociation constant (Eq. 1)[16]:

$$\left(\frac{\partial \ln K_{\mathrm{D}}}{\partial \pi}\right) = \frac{\Delta V}{RT} \qquad \text{(Eq. 1)}$$

where K_{D} is the dissociation constant, π is the osmotic pressure, ΔV is the partial molar volume change, R is the gas constant, and T is the absolute temperature.

Although the partial volume change can be readily calculated from the osmotic pressure dependence of K_{D}, estimating K_{D} for the ET complex is not simple. The redox states of the two proteins change immediately after complex formation, which prevents us from estimating the K_{D} for the "active" and transiently formed ES complex comprising Cyt *c* and C*c*O. Fluorescence quenching[18] or other spectroscopic techniques[19] can be used to determine the K_{D} for the formation of the complex between oxidized Cyt *c* and fully oxidized C*c*O or between reduced Cyt *c* and fully reduced C*c*O, whereas determining K_{D} for the ES complex between reduced Cyt *c* and the oxidized C*c*O is impossible due to the ET reaction within the complex. On the other hand, steady-state kinetic analysis for the aerobic oxidation of reduced Cyt *c* catalyzed by C*c*O can determine the stability of the ES complex as K_{M}, Michaelis constant. K_{M} is often treated as K_{D}, although K_{M} is not the dissociation constant, K_{D}, for the ES complex. The steady-state kinetic properties of the C*c*O reaction have shown that oxidized Cyt *c* functions as a competitive inhibitor to reduced Cyt *c* and that the K_{D} of the enzyme-oxidized Cyt *c* complex (or the enzyme-inhibitor

complex) is identical to K_M[20]. These kinetic properties strongly suggest that K_M determined by the steady-state kinetic analysis essentially corresponds to K_D of the ES complex, as described in detail in the section of Discussion.

MATERIALS AND METHODS

Protein Expression and Purification. Wild-type and mutant Cyt *c* proteins were expressed and purified according to our published procedures[4, 21]. The *E. coli* strain Rosetta 2(DE3)pLysS cells transformed with the plasmids containing the DNA of Cyt *c*[22] were inoculated in 5 mL of a 2xTY medium and grown overnight. This pre-cultured medium was added to 4 L of a 2xTY medium and the bacteria were further incubated at 37°C. The expression of Cyt *c* was initiated by adding 0.8 mM IPTG to the culture when the cell density reached an absorbance of 0.6 at 600 nm. And then 0.1 mM δ-aminolevulinic acid was added to promote heme biosynthesis. After additional incubation for 24 hours, the cells were collected by centrifugation.

The cell pellet was resuspended in 50 mM Tris-HCl at pH 7.5 containing 1 g/L lysozyme, 50 mg/L DNase I, and 50 mg/L RNase A and suspended for 3 hours to lyse the cell pellet completely at 4˚C. The supernatant of the crude extract was obtained by centrifugation at 25,000 × g for 30 minutes and 125,000 × g for 1 hour at 4˚C. This supernatant was purified by HiPrep 16/10 SP HP column (GE Healthcare) with a linear salt gradient of 1 - 300 mM NaCl. The elution sample was concentrated by amicon ultrafiltration using 5 kDa cut-off membranes. To completely oxidize Cyt *c*, concentrated Cyt *c* was stirred for 1 hour with 10-fold potassium ferricyanide. After Cyt *c* was dissolved into 50 mM sodium phosphate buffer at pH 7.0, Cyt *c* was further purified by Mono S 10/100 GL column (GE Healthcare) with a linear salt gradient. The purified Cyt *c* fractions

were pooled, concentrated, and applied to HiLoad 16/60 Superdex 75 gel filtration column (GE Healthcare).

Mutagenesis was conducted utilizing the PrimeSTAR mutagenesis basal kit from Takara Bio (Otsu, Japan). DNA oligonucleotides (Table S1) were purchased from Operon Biotechnologies (Tokyo, Japan). The mutated genes were sequenced (Operon Biotechnologies, Tokyo, Japan) to ensure that the desired mutations were introduced.

C*c*O was purified from bovine heart as described previously[23] and dissolved into the 50 mM sodium phosphate buffer at pH 6.8 containing 0.1 % *n*-decyl-β-D-maltoside.

Selection of Osmolytes. The osmotic pressure, π, for the solvent at different osmolyte concentration was estimated using Eq.2,

$$\pi = -\frac{RT}{V_{\mathrm{H_2O}}} \times \ln X_{\mathrm{H_2O}} \qquad \text{(Eq. 2)}$$

where X_{H2O} and V_{H2O} are the molar fraction and the molar volume of water, respectively. X_{H2O} was calculated using tabulated values of the water content for each osmolyte/water mixtures[24]. For V_{H2O}, a value of 18 mL mol^{-1} was used.

We used four kinds of osmolytes, sucrose, D-glucose, glycerol, and ethylene glycol, to increase the osmotic pressure, and previous studies have shown that these sugars and polyalcohols have no specific interactions with proteins[25, 26]. By addition of one of these osmolytes, no significant spectral perturbations were induced in the absorption spectra of Cyt *c* (Figure S5). However, addition of the osmolytes increases the viscosity of the solutions, and the increased viscosity substantially perturbs the protein-protein complex formation [27]. Such perturbations

induced by the viscosity was encountered for the binding of a restriction enzyme, *Eco*RV, to the target DNA sequence[28]. The osmotic pressure dependence of K_M for the DNA cleavage reaction by *Eco*RV was substantially affected by the viscosity of the solution containing osmolyte. In the ET reaction from Cyt *c* to C*c*O, the combined effect of viscosity and osmotic pressure on K_M in the presence of various kinds of glycerol concentrations was rather modest (Figure S3) as previously suggested[27]. Such a modest perturbation of K_M was also observed by varying the solution viscosity under the constant osmotic pressure (Figure S4) due to the delay of the protein translational diffusion[29]. To avoid the effects of viscosity on the complex formation, we determined the concentration of osmolyte so that the viscosity of the solution is constant (summarized in Table S2). The value of the viscosity for each osmolyte/water mixture was cited from *CRC Handbook of Chemistry and Physics*[24]. At the constant viscosity of the solution (1.6 mPa・s), the electron transfer reactions were followed to estimate the K_M values.

Measurements of Electron Transfer Activity of Cyt *c* under Initial Steady-State Conditions. The electron transfer reaction from Cyt *c* to C*c*O was measured with a Hitachi U-3310 UV-visible spectrophotometer at 293 K in 50 mM NaPi/NaOH containing one of the osmolytes listed in Table S2, pH 6.8, 0.1% *n*-decyl β-D-maltoside, as previously reported[7]. The detailed compositions of the reaction medium are also summarized in Table S2. Ferrous Cyt *c* was prepared by the reduction of ferric Cyt *c* with dithionite and excess reductant was removed by a PD MiniTrap G-25 column[7]. The concentrations of Cyt *c* varied between 0.5 and 40 μM, and oxidation of Cyt *c* was followed by the absorbance at 550 nm after adding C*c*O to the reaction solution at the final concentration of 1 nM. The absorption at 550 nm was recorded with an interval of 1 s for 3 minutes. To determine the end point of the electron transfer reaction from Cyt *c* to C*c*O, a small amount of potassium ferricyanide (III) was added to the reaction solution, as shown in

Figure S1A (downward arrow). The first order oxidation of reduced Cyt *c* was observed as shown in Figure S1B and Eq. 3, as reported in the previous papers[30, 31].

$$\upsilon = -\frac{d[\mathrm{Cyt}\,c^{2+}]}{dt} = k_{\mathrm{obs}}[\mathrm{Cyt}\,c^{2+}] \qquad \text{(Eq. 3)}$$

where υ is the oxidation rate of reduced Cyt *c*, and k_{obs} is the apparent rate constant at the various concentrations of Cyt *c*. Therefore, k_{obs} can be estimated by the following equation:

$$\ln[\mathrm{Cyt}\,c^{2+}] = -k_{\mathrm{obs}}t + \ln[\mathrm{Cyt}\,c^{2+}]_0 \qquad \text{(Eq. 4)}$$

In this equation, the concentration of Cyt c^{2+}, [Cyt c^{2+}], can be determined by the absorbance change at 550 nm as follows:

$$[\mathrm{Cyt}\,c^{2+}] = \Delta\mathrm{Abs}_{550}/\varepsilon \qquad \text{(Eq. 5)}$$

where ε is the difference of the extinction coefficients between reduced and oxidized Cyt *c* at 550 nm. By using Eq. 4 and Eq. 5, k_{obs} can be estimated from the absorbance change at 550 nm by the following equation (Figure S1B):

$$\ln \Delta\mathrm{Abs}_{550} = -k_{\mathrm{obs}}t + \ln\varepsilon + \ln[\mathrm{Cyt}\,c^{2+}]_0 \qquad \text{(Eq. 6)}$$

Consistent with previous reports[30, 31], a single rectangular hyperbolic relationship between υ and [Cyt c^{2+}]$_0$ was obtained under the present experimental conditions, as given in Eq. 7.

$$\upsilon = \frac{V_{\mathrm{max}}[\mathrm{Cyt}\,c^{2+}]_0}{K_{\mathrm{M}} + [\mathrm{Cyt}\,c^{2+}]_0} \qquad \text{(Eq. 7)}$$

We estimated the Michaelis-Menten parameters using [Cyt c^{2+}] and k_{obs}, which is determined by Eq. 6. The turnover number, k_{cat}, was calculated by using the following equation:

$$k_{cat} = \frac{V_{max}}{[C\mathit{c}O]} \quad \text{(Eq. 8)}$$

where [C*c*O] denotes the total enzyme concentration.

Molecular Docking of Mutant Cyt *c* with C*c*O. We predicted the ET complex between the I81S Cyt *c* mutant and C*c*O by using the molecular docking simulation we examined in a previous paper[7]. The initial geometry of the I81S mutant was constructed from the wild-type complex by replacing the side chain of Ile81 in the wild-type protein with Ser and energetically minimized the protein according to our previous procedure[7].

Based on the predicted complex structure between the I81S Cyt *c* mutant and C*c*O, we estimated the binding free energy of Cyt *c* with C*c*O (ΔG_{bind}) and that for the dehydration from the protein surface associated with complex formation (ΔG_{sol}). ΔG_{bind} consists of the energy and entropy terms, and the energy term can be further divided into three terms, internal energy (ΔE_{int}), van der Waals energy (ΔE_{vdW}), and Coulombic energy (ΔE_{coul}). Among them, the contribution of the entropy term and ΔE_{int} to ΔG_{bind} are quite small compared to other two terms[32]. ΔE_{vdW} and ΔE_{coul} are primary factors to determine ΔG_{bind}. On the other hand, we calculated ΔG_{sol} based on an implicit continuum solvation model using Poisson-Boltzmann equation, which is the sum of the free energy for polar interactions (ΔG_{polar}) and the nonpolar interactions ($\Delta G_{nonpolar}$). As found in most protein-protein complex formation systems[33], ΔE_{coul} is compensated for by ΔG_{polar} and there is an anti-correlation between these two energies. Consequently, the variance of the sum of

electrostatic contributions ($\Delta G_{electro} = \Delta E_{coul} + \Delta G_{polar}$) is significant as well as the variance of hydrophobic interactions, ΔE_{vdW} and $\Delta G_{nonpolar}$.

RESULTS

Osmotic Pressure Dependence of Michaelis Constant for ES complex between Cyt *c* and C*c*O. To investigate the dehydration associated with the formation of Cyt *c* with C*c*O, we determined the K_M values under various osmotic pressure by the steady-state kinetics for the ET from Cyt *c* to C*c*O. The initial steady-state rates determined from the time course indicate a simple Michaelis-Menten relationship (Figures S1 and S2), namely, a single Cyt *c*-binding model under the present pH and ionic strength conditions, consistent with a previous report[31]. The kinetics results were, therefore, analyzed using the simple Michaelis-Menten equation[34].

As described in Materials and Methods, the osmotic pressure of the protein solution was increased by the addition of sugars or polyalcohols that have no specific interactions with proteins[25, 35, 36]. Although recent study reported that high concentration (40%) of ethylene glycol increased the K_M value for the ET reaction from Cyt *c* to C*c*O by a factor of approximately 5, suggesting that ethylene glycol could directly perturb the configuration of the Cyt *c* – C*c*O complex and function as a competitive inhibitor of the steady-state reaction[37]. In this paper, however, the concentration of the osmolyte we used was less than 20%, and no significant changes in the absorption spectra of Cyt *c* were confirmed before the kinetic measurements in the presence of ethylene glycol (Figure S5). In fact, the K_M value in the presence of 18.6% ethylene glycol was 0.80 ± 0.11 μM (Figure 1), which was smaller than that in the presence of 7.14% ethylene glycol (0.825 ± 0.059 μM, Figure S4) and in the absence of the osmolyte (1.2 ± 0.1 μM) [7]. Less than

20% ethylene glycol is, therefore, unlikely to induce configurational changes of the Cyt *c* – C*c*O complex to increase the K_M value for the ET reaction from Cyt *c* to C*c*O. The K_M values at various osmotic pressures are summarized in Table 1. As Table 1 clearly shows, the K_M value decreased with increasing osmotic pressure, corresponding to the negative volume change (Eq. 1). It should be noted here that the addition of the osmolyte decreases the water activity, which suppresses the ionization of NaPi in solutions and results in the decreased ionic strength of the reaction medium (Table S2). Such a decrease in the ionic strength by the addition of the osmolyte was, however, less than 3 mM. Perturbations in the water activity induced by the addition of the osmolyte would, therefore, not significantly affect the K_M values under the conditions we followed the ET reactions.

To calculate the volume change associated with the formation of the Cyt *c* – C*c*O complex, the K_M value was plotted against the osmotic pressure, as shown in Figure 1. Based on the slope of the fitting line for wild-type Cyt *c* (WT: red) in Figure 1, the partial volume change was negative and estimated to be -314 ± 50 mL mol^{-1} (Table 2), implying that dehydration was induced during complex formation. Given the assumption that the volume change for dehydration from hydrophobic amino acid residues is -17.5 mL mol^{-1}[38], the volume change we obtained here corresponds to dehydration involving 17 ± 3 water molecules. On the other hand, assuming that the number of the released hydration water molecules simply depends on the area of the interaction site[39, 40], the interaction area estimated by our NMR experiments[4] (~1800 $Å^2$) suggests that nearly 100 water molecules can be expelled from the interaction site. A much smaller number of released hydration water molecules estimated by the osmotic pressure experiments (< 20 water molecules) suggests that the number of direct interactions of amino acid residues that induce dehydration is much less than that we expected from the NMR measurement. The smaller number of released hydration water molecules associated with complex formation is also supported by the

crystal structure of the complex between Cyt *c* and C*c*O[8]. The interface between the two proteins is loosely packed and three water layers with a long-molecular span are formed in the interface[8], which is sufficient for many hydrating water molecules to remain around the amino acid residues in the interaction site at the Cyt *c* – C*c*O protein-protein interface and consistent with our recent results from the docking simulation[7].

The comparison of the crystal structure of the Cyt *c* – C*c*O complex (PDB: 5IY5)[8] with those of unbound Cyt *c* (PDB: 3ZCF)[41] and C*c*O (PDB: 2DYR)[42] also suggests that the dehydration is associated with complex formation. Analysis of the electron density map of these crystal structures at different sigma levels[43] revealed that the number of hydration water molecules located within 3.5 Å from the nearest atom of the interacting residues of Cyt *c* with C*c*O[4] was estimated to be 21 (1.5 σ) or 16 (2.0 σ), respectively, and that of C*c*O with Cyt *c*[7] was 38 (1.5 σ) or 32 (2.0 σ), respectively. By the complex formation between Cyt *c* and C*c*O, the number of the hydration water molecules in the Cyt *c* surface of the complex is decreased to 15 (1.5 σ) or 7 (2.0 σ), respectively, showing that 6 – 9 hydration molecules are released from the surface of Cyt *c*. Such release of hydration water molecules is also encountered for the surface of C*c*O. The complexation with Cyt *c* expels 2 – 7 hydration water molecules from the surface of C*c*O. Based on the comparison of these crystal structures, 8 – 16 hydration water molecules at the Cyt *c* and C*c*O surfaces in the interaction site would be dehydrated by the complexation, which is consistent with our estimation of the decrease of the hydration water molecules based on the osmotic pressure experiments.

Dehydration Sites for Cyt *c* – C*c*O Complexation. To identify the dehydration sites in the interface between C*c*O and Cyt *c*, we focused on hydrophobic amino acid residues in the C*c*O

interaction site on Cyt *c* and mutated one of the hydrophobic amino acid residues to examine the osmotic pressure effects on K_M for complex formation. As we previously reported[4], three isoleucine residues, Ile9, Ile11, and Ile81, are located in the interaction site (Figure S6). The exposed surface areas of the side chains[44] (Table S3) indicate hydration by 1, 4, and 7 water molecules around the side chains of Ile9, Ile11, and Ile81, respectively. We replaced each Ile with Ala, which has a smaller hydrophobic side chain and fewer hydrating water molecules around the side chain, and measured the Cyt *c* oxidation reaction at various osmotic pressures. As we recently reported[7], these mutations at the interaction site induce only localized structural changes and the structures of mutant Cyt *c* are quite similar to that of the wild-type protein, confirming that the mutations affect only the hydration of water molecules at the mutation site. Tables S4 and S5 summarize the obtained Michaelis-Menten kinetic parameters of the wild-type and mutant proteins.

As clearly illustrated in Figure 1, the slope of the osmotic pressure dependence of the K_M for the Ile mutants is less steep than that for the wild-type protein except for the Ile9 mutant (Table S4). The estimated volume changes for complex formation are -246 ± 72, -197 ± 38, -139 ± 38 mL mol^{-1} for the Ile11 → Ala, Ile81 → Ser and Ile81 → Ala mutants, respectively. The decreased volume changes in the Ile mutants imply that the number of water molecules released during dehydration was reduced to 14 ± 4, 11 ± 3 and 8 ± 2 due to the mutations of Ile11 → Ala, Ile81 → Ser and Ile81 → Ala, respectively. Although the decreased number of dehydrated water molecules for the Ile11 mutant is within the experimental error, the reduced numbers of water molecules involved in dehydration in the Ile81 mutants are significant. This result indicates that the hydrating water molecules around Ile81 are expelled to the solvent during formation of the ET complex between Cyt *c* and C*c*O. In particular, approximately 10 water molecules are released during the

dehydration of Ile81, which allows us to conclude that Ile81 is the primary dehydration site for complex formation between Cyt *c* and C*c*O under the turnover conditions.

In sharp contrast to the mutations at Ile81, the mutations at lysine residues in the interaction sites were less effective for decreasing the number of dehydrated water molecules (Figure 1, Table 2 and Table S4). We have revealed that Lys13 is involved in the key interaction with C*c*O[4] and it has many hydrophobic methylene groups in the long side chain, but the number of dehydrated water molecules decreased by less than 5 upon the substitution of Ala for Lys13. The mutation of Lys79, which is located adjacent to Ile81, also induced a minor perturbation to dehydration. The comparable number of dehydrated water molecules in the Lys mutant relative to that in the wild-type protein also supports the preferential and specific dehydration from Ile81 in formation of the transient ET complex between Cyt *c* and C*c*O.

Thermodynamic Analysis of Association of Cyt *c* with C*c*O. To examine functional significance of the release of 10 water molecules during the dehydration of hydrophobic amino acid residues, we focused on the thermodynamic contribution of dehydration to ET complex formation and determined the enthalpy (ΔH) and entropy (ΔS) for the complex formation between Cyt *c* and C*c*O. Based on the temperature dependence of K_M for the steady-state kinetics of the ET reaction from Cyt *c* to C*c*O (van't Hoff plot analysis) (Figures 2 and S7, Michaelis-Menten kinetic parameters are listed in Tables S6 and S7), ΔH and ΔS for complex formation in wild-type Cyt *c* were determined to be 13.0 ± 1.6 $kJmol^{-1}$ and 161 ± 6 $JK^{-1}mol^{-1}$, respectively (Figure 2, closed circle and Table 3). These obtained values indicate that complex formation between Cyt *c* and C*c*O is an energetically unfavorable and entropy-driven reaction. After mutation of Ile81 to Ala, the plots of ln K_M versus $1/T$ (Figure 2, closed square) are completely different from those of the wild-

type protein, which presents a negative ΔH (- 3.53 ± 3.01 kJmol^{-1}) and reduced ΔS (103 ± 10 JK^{-1}mol^{-1}). The introduction of a more hydrophilic residue—Ser—into the Ile81 position resulted in a more negative ΔH (- 14.9 ± 1.4 kJmol^{-1}) and smaller ΔS (72 ± 5 JK^{-1}mol^{-1}) (summarized in Table 3). The complex formation between Ile81-mutated Cyt *c* and C*c*O is an energetically favorable reaction and the contribution of entropy to the thermal stability of the complex was reduced in the Cyt *c* mutant. Such reduced contribution of entropy to complex formation in the I81A mutant ($\Delta\Delta S_{I81A\text{-}WT} = \Delta S_{I81A} - \Delta S_{WT}$ = - 58 JK^{-1}mol^{-1}) can be contributed to the decreased number of hydration water molecules released from the protein surface around position 81, assuming that the mutation at Ile81 does not affect the entropy changes for the overall rotational and translational degrees of freedom and the conformational changes of the proteins associated with the Cyt *c* – C*c*O complex formation.

To get further insights into the energetic contribution of each amino acid residue to the complex formation between Cyt *c* and C*c*O, the structure of the ET complex between the I81S Cyt *c* mutant and C*c*O was predicted by using molecular docking simulation as previously reported[7]. Based on the predicted complex structure, we estimated the free energy change for the formation of hydrophobic interaction (ΔE_{vdW}) for the binding of Cyt *c* with C*c*O and those for the dehydrations from hydrophobic ($\Delta G_{nonpolar}$) and charged ($\Delta G_{electro}$) protein surface associated with the complex formation (Figure 3). The validity of the energy calculation was confirmed by the total free energy change ($\Delta G_{tot} = \Delta G_{bind} + \Delta G_{sol}$) for the complexation; the calculated ΔG_{tot} for the I81S mutant was - 8.51 kcal mol^{-1}, which is in good agreement with the experimental value (- 8.60 kcal mol^{-1}) calculated for the thermodynamic parameter in Table 3. One of the significant perturbations induced by this mutation is enhancement of the favorable electrostatic interactions ($\Delta G_{electro}$) in Lys72 (- 6.86 and - 5.17 kcal mol^{-1} for I81S and wild-type Cyt *c*, respectively) and

Lys79 (- 6.91 and - 5.64 kcal mol^{-1} for I81S and wild-type Cyt *c*, respectively). These enhanced electrostatic interactions suggest that there are more polar environments around Lys72 and Lys79 in the I81S mutant, compared with those in the wild-type protein. Another significant change in the energy profile of the I81S mutant is the increased unfavorable electrostatic interaction of Val83 and Glu90. Val83 is one of the hydrophobic amino acid residues near the exposed heme periphery and the free energy for the dehydration ($\Delta G_{electro}$) was positively shifted from 0.68 kcal mol^{-1}[7] to 2.16 kcal mol^{-1} (Figure 3) by the mutation of Ile to Ser at position 81. Although Glu90 is far from the exposed heme periphery and the energetic contribution to the complex formation between wild-type Cyt *c* and C*c*O was rather small (less than 3 kcal mol^{-1})[7], the significant unfavorable electrostatic energy at Glu90 (3.90 kcal mol^{-1}) was detected in the I81S mutant. These findings suggest that the mutation at position 81 induced significant perturbation of the binding orientation of Cyt *c* to C*c*O, which is supported by the predicted complex structure between the I81S Cyt *c* mutant and C*c*O (Figure S8(a)). As illustrated in Figure 4, the distribution of amino acid residues forming hydrophobic interactions to stabilize the ET complex between Cyt *c* and C*c*O is significantly perturbed in the I81S Cyt *c* mutant.

DISCUSSION

Significance of Michaelis Constant, K_M, Determined by Steady-State Kinetic Analysis. It has been well established that a rectangular hyperbolic relationship between the enzyme activity and [Cyt c^{2+}] as given in Eq. 7 is detectable under the present experimental conditions (Cyt c^{2+} oxidation by a catalytic amount of C*c*O under the initial steady-state conditions) and that this steady-state kinetic system shows the first order oxidation of Cyt c^{2+} and the competitive inhibition

of Cyt c^{3+} against the binding of Cyt c^{2+} to C*c*O[20, 45, 46]. The above rectangular hyperbolic relationship as given by Eq. 7 indicates, at least apparently, that a single electron equivalent from Cyt c^{2+} reduces one equivalent of molecular oxygen to produce two water molecules. Discussion on this apparent discrepancy, which has not been done in detail thus far, would be helpful to understand the significance of the experimentally determinable parameters (V_{max} and K_M).

The rectangular hyperbolic relationship indicates a steady-state kinetic model as given in Figure 5, which implies four discrete electron transfer events to provide four different intermediate species of C*c*O, designated as E, F, G and H in Figure 5. The kinetic model given in Figure 5 provides the following initial steady state equation

$$\frac{\upsilon}{[\mathrm{C}c\mathrm{O}]} = \frac{[\mathrm{S}]}{\left\{\left(\frac{K_\mathrm{M}^1 + [\mathrm{S}] + (K_\mathrm{M}^1/K_\mathrm{i}^1)[\mathrm{P}]}{k_3}\right) + \left(\frac{K_\mathrm{M}^2 + [\mathrm{S}] + (K_\mathrm{M}^2/K_\mathrm{i}^2)[\mathrm{P}]}{k_8}\right) + \left(\frac{K_\mathrm{M}^3 + [\mathrm{S}] + (K_\mathrm{M}^3/K_\mathrm{i}^3)[\mathrm{P}]}{k_{13}}\right) + \left(\frac{K_\mathrm{M}^4 + [\mathrm{S}] + (K_\mathrm{M}^4/K_\mathrm{i}^4)[\mathrm{P}]}{k_{18}}\right)\right\}} \quad \text{(Eq. 9)}$$

where S and P denote Cyt c^{2+} and Cyt c^{3+}, respectively, and $K_\mathrm{M}^1 = \frac{k_2 + k_3}{k_1}$, $K_\mathrm{M}^2 = \frac{k_7 + k_8}{k_6}$, $K_\mathrm{M}^3 = \frac{k_{12} + k_{13}}{k_{11}}$, $K_\mathrm{M}^4 = \frac{k_{17} + k_{18}}{k_{16}}$, $K_\mathrm{i}^1 = \frac{k_5}{k_4}$, $K_\mathrm{i}^2 = \frac{k_{10}}{k_9}$, $K_\mathrm{i}^3 = \frac{k_{15}}{k_{14}}$, and $K_\mathrm{i}^4 = \frac{k_{20}}{k_{19}}$. The numbers of the rate constants are as given in Figure 5. The rate constants, k_3, k_8, k_{13} and k_{18} are those of the release of Cyt c^{3+}. This equation shows a rectangular hyperbolic relationship between the activity and [Cyt c^{2+}], as given in Eq. 7 and the competitive inhibitor function of Cyt c^{3+} against Cyt c^{2+}. Furthermore, when $K_\mathrm{M}^1 = K_\mathrm{i}^1$, $K_\mathrm{M}^2 = K_\mathrm{i}^2$, $K_\mathrm{M}^3 = K_\mathrm{i}^3$, and $K_\mathrm{M}^4 = K_\mathrm{i}^4$, Eq. 9 becomes Eq. 10, as follows

$$\frac{\upsilon}{[\mathrm{C}c\mathrm{O}]} = \frac{[\mathrm{S}]}{\left\{\left(\frac{K_\mathrm{M}^1 + [\mathrm{S}] + [\mathrm{P}]}{k_3}\right) + \left(\frac{K_\mathrm{M}^2 + [\mathrm{S}] + [\mathrm{P}]}{k_8}\right) + \left(\frac{K_\mathrm{M}^3 + [\mathrm{S}] + [\mathrm{P}]}{k_{13}}\right) + \left(\frac{K_\mathrm{M}^4 + [\mathrm{S}] + [\mathrm{P}]}{k_{18}}\right)\right\}} \quad \text{(Eq. 10)}$$

The denominator of Eq. 10 depends on the total concentration of Cyt *c* irrespective of the ratio of [Cyt c^{2+}] to [Cyt c^{3+}]. Thus, in each enzyme assay measuring oxidation of Cyt c^{2+}, the constant denominator provides the first order oxidation of Cyt c^{2+}, as described by Eq. 3. Thus, the first order oxidation of Cyt c^{2+} indicates that the K_M value of each intermediate species is identical to its K_i value. In fact, Yonetani and Ray reported that significant deviation from the first order oxidation process was detectable when K_M was not identical to K_i under significantly alkaline conditions[20].

The experimentally obtainable parameters, K_M and k_{cat}, can, therefore, be written as follows

$$K_M = \frac{K_M^1/k_3 + K_M^2/k_8 + K_M^3/k_{13} + K_M^4/k_{18}}{1/k_3 + 1/k_8 + 1/k_{13} + 1/k_{18}} \quad \text{(Eq. 11)}$$

$$k_{cat} = \frac{1}{1/k_3 + 1/k_8 + 1/k_{13} + 1/k_{18}} \quad \text{(Eq. 12)}$$

It should be noted that K_M^1, K_M^2, K_M^3, and K_M^4 are equal to K_i^1, K_i^2, K_i^3, and K_i^4, respectively. Eq. 11 indicates that the experimentally obtainable parameter K_M is the average of the microscopic K_M values for the four intermediate species, weighted by the relative rates of the product (or Cyt c^{3+}) release.

In general, K_M is not K_D for ES complex in the Michaelis-Menten system, namely, K_M is not a thermodynamic parameter. However, in the present steady-state kinetic system of C*c*O, K_M of each electron transfer step is identical to K_i of the electron transfer step. For example, in the initial step in Figure 5, two binding reactions proceed:

$$E + S \underset{k_2}{\overset{k_1}{\rightleftharpoons}} ES \xrightarrow{k_3} F + P \quad , K_M^1 = \frac{k_2 + k_3}{k_1}$$

$$E + P \underset{k_5}{\overset{k_4}{\rightleftharpoons}} EP \quad , K_i^1 = \frac{k_5}{k_4}$$

where E is C*c*O, S is reduced Cyt *c*, P is oxidized Cyt *c*, and F is reduced C*c*O. While the steady-state kinetic results indicate $K_i^1 = K_M^1$, the NMR analysis for interactions between Cyt *c* and C*c*O revealed that the interaction site for C*c*O in oxidized Cyt *c* was almost overlapped with that in reduced Cyt *c*[4], supporting the assumption that the overall affinity of oxidized Cyt *c* for C*c*O is equal to that of reduced Cyt *c*, namely $k_5/k_4 = k_2/k_1$. These observations suggest that K_M^1 can be considered as the dissociation constant, K_D^1 (= k_2/k_1) for the ES complex in Figure 5. In other words, the K_M of each step can be treated as the K_D of the ES complex in the step. The experimentally obtainable parameter, K_M, is the weighted average of the microscopic K_D values for the four intermediate species. Thus, the K_M, obtained under the present conditions can be treated as a thermodynamic parameter. Although stable C*c*O forms including various inhibitor-bound forms[46], the fully reduced form and the fully oxidized form as isolated[47] have been often used as models of the unstable catalytic intermediate species under the turnover conditions[46], they are not directly involved in the catalytic cycle . It is, therefore, noteworthy that the present and previous[7] works have introduced a new approach for characterization of enzyme species under turnover conditions using the initial steady-state kinetics.

Energetic Contribution of Dehydration to Complex Formation between Cyt *c* and C*c*O. As clearly shown in Figure 1 and Table 2, the osmotic pressure dependence of K_M for the ET reaction from Cyt *c* to C*c*O revealed that approximately 20 hydration water molecules were expelled to the bulk upon the complex formation between Cyt *c* and C*c*O. By mutation of Ile81 to Ala, the number of hydration water molecules released upon the complex formation is decreased from 17 ± 3 to 8 ± 2, implying that approximately 10 water molecules would still be hydrated in

the complex between I81A Cyt *c* mutant and C*c*O. Because the entropy change for dehydration involving one water molecule and a hydrophobic amino acid residue was estimated to be 5.5 $JK^{-1}mol^{-1}$[48], the entropy change due to dehydration involving 10 water molecules corresponds to approximately 60 $JK^{-1}mol^{-1}$, which is comparable to $\Delta\Delta S_{I81A\text{-}WT}$ from Table 3**.** Considering that the entropy change due to the reductions in the overall rotational and translational degrees of freedom associated with the formation of a protein-protein complex, which is one of the major entropy change in protein-protein complex formation, is – 33.5 $JK^{-1}mol^{-1}$[49], thermodynamic contribution from dehydration around Ile81 (~ 60 $JK^{-1}mol^{-1}$) is significant. This contribution compensates for the reduced entropy due to complex formation and the dehydration is one of the major factors that increases the entropy during complex formation.

Functional Significance of Dehydration to Electron Transfer from Cyt *c* to C*c*O. The most remarkable finding of this work is that the primary dehydration site during the formation of the Cyt *c* – C*c*O complex is located near a hydrophobic area including a hydrophobic thioether group (Figure S6) in Cyt *c*. The electron entry site for C*c*O, the Cu_A site, is also in the hydrophobic region constructed by several aromatic amino acid residues on the protein surface of C*c*O[23]; thus, the dehydration results in induction of interactions involving the hydrophobic area around the exposed heme periphery of Cyt *c* and the hydrophobic region of C*c*O. Our previous energetic analysis revealed the distribution of amino acid residues mediating hydrophobic interactions between Cyt *c* and C*c*O[7]. As shown in Figure 4(a), amino acid residues showing relatively large free energy for hydrophobic interactions, ΔE_{vdW} and $\Delta G_{nonpolar}$, surround the exposed heme periphery, acting as a "molecular breakwater" to inhibit the invasion of the bulk water molecules to the hydrophobic interaction site around the exposed heme periphery of Cyt *c* and the hydrophobic region of C*c*O. The hydrophobic methylene groups (-CH_2-) of the side chain of

charged or hydrophilic amino acid residues including Lys13, Gln16, Lys27, and Thr28 also contribute to the formation of the hydrophobic interactions. These amino acid residues surrounding the redox centers supports the function of nearby solvent-exposed hydrophobic residues such as Ile81 by dehydrating water molecules around the redox centers for formation of the "molecular breakwater", which inhibits the exchange of water molecules between the sterically constrained ET region and the more turbulent surrounding bulk water molecules[50]. Such hydrophobic interactions surrounding the redox center are also encountered for other ET complexes[50-52], suggesting that the "molecular breakwater" inhibits the invasion of bulk water molecules to form nonspecific hydrogen bonds around the protein-protein interaction sites, which is likely to form alternative ET pathways and reduce the specificity of the ET reaction.

The introduction of a hydrophilic residue into the "molecular breakwater" by mutation of Ile81 to Ser was found to affect the energetic contributions of the amino acid residues to the complex formation between Cyt *c* and C*c*O as shown in Figure 3. The amino acid residues in Cyt *c* interacting with C*c*O were significantly perturbed in the mutant, but the interaction site of the mutant was also located near the exposed hydrophobic periphery, as observed for wild-type Cyt *c*. Although the interface between Cyt *c* and C*c*O in the X-ray structure has more space than that of the simulated complex structure, the X-ray structure also indicates that the hydrophobic heme periphery is involved in the interaction site of Cyt *c* to C*c*O, supporting the simulated complex structure. As described in the section of RESULTS, introduction of a hydrophilic amino acid residue, Ser, into the position of Ile81 resulted in more polar environments around Lys72 and Lys79. The decreased hydrophobicity around Lys79, located adjacent to residue 81 and the exposed hydrophobic heme periphery (Figure S6), would weaken the effects of the "molecular breakwater" to protect the hydrophobic interaction site from bulk water molecules. The enhanced

unfavorable electrostatic interaction for the complex formation was detected at Val83, one of the surrounding amino acid residues constructing the "molecular breakwater" around the exposed hydrophobic heme periphery, in the I81S mutant. The decreased stabilization energy at Val83 would also result in a weakened "molecular breakwater". As illustrated in Figure 4, the distribution of amino acid residues forming hydrophobic interactions to stabilize the ET complex between Cyt *c* and C*c*O is significantly perturbed in the I81S Cyt *c* mutant, and the distribution of the "molecular breakwater" in the mutant has a gap around position 81.

Although the hydrophobic interactions were weakened in the complex between the I81S Cyt *c* mutant and C*c*O, a new hydrogen bond between Ser81 of the I81S Cyt *c* mutant and Glu157 in Subunit II of C*c*O was formed (Figure S8(b)), which also contributes to the reduced hydrophobicity of the interaction site of the mutant. The formation of the hydrogen bond reduced the repulsive electrostatic interaction by Glu157 in Subunit II of C*c*O (+ 6.2 and $< + 3$ kcal mol^{-1} in wild-type Cyt *c* and the I81S mutant, respectively)[7], thus supporting the enthalpy-driven complex formation between the I81S Cyt *c* mutant and C*c*O and not the entropy-driven formation observed for wild-type Cyt *c* (Table 3). While hydrogen bonds are efficient ET mediators in proteins[53], the k_{cat} value of the I81S mutant at 293 K was 96.0 ± 1.7 s^{-1} (Figure S7C), which is significantly slower than that of the wild-type protein under the same conditions (119 ± 4 s^{-1}) (Table S7). Thus, the newly formed hydrogen bond between Ser81 in Cyt *c* and Glu157 in subunit II of C*c*O would not contribute to formation of a more effective ET pathway and the reduced hydrophobicity in the interface between Cyt *c* and C*c*O as discussed above would decrease the efficiency of the ET process.

Therefore, the simulation analysis for the Ile81 mutation revealed decreased hydrophobic interactions and increased electrostatic interactions in the interface between Cyt *c* and C*c*O due to

the introduction of the hydrophilic amino acid residue Ser into position of 81. The decreased dehydration around Ser81 was also confirmed by the reduced entropy required for the I81S mutant to form the ET complex with C*c*O (Figure 2 and Table 3). These observations strongly support the primary contribution of the dehydration from Ile81 to the formation of the "molecular breakwater" upon Cyt *c* – C*c*O complex formation during catalytic turnover. The present analyses also suggest that once the breakwater is broken by the mutation, water molecules around the redox centers are not effectively expelled and bulk solvent molecules penetrating into the redox centers perturb the interaction site of Cyt *c* for C*c*O which forms the ET pathway from Cyt *c* to C*c*O.

In conclusion, by measuring the steady-state kinetics at various osmotic pressures, we successfully determined the number of water molecules released during the dehydration of hydrophobic amino acid residues in the C*c*O – Cyt *c* interaction site. The present extensive mutational analysis has identified the hydrophobic region near the exposed heme periphery region as the major dehydration site in Cyt *c*. The present results suggest that such dehydration is a primary factor to increase the entropy for the formation of the Cyt *c* – C*c*O complex, which contributes to the formation of the hydrophobic ET pathway and suppress the formation of hydrogen bond-mediated nonspecific ET pathways, thus promoting effective and specific ET from Cyt *c* to C*c*O.

Funding

This work was supported by Grants-in-aid 25288072 and 25109501 (to K. I.), 26234567 (to S. Y.), and 24109014 and 15K13710 (to K. Y.) from the Japan Society for the Promotion of Science.

Declaration of interest

The authors declare no competing financial interest.

Author Contributions

W.S. and K.I. designed research. W.S. and K.S-I. performed experiments. W.S., T.U., and K.I. analyzed data. S.H. and K.Y conducted the simulations and analyzes. W.S., S.Y., and K.I. wrote the article.

REFERENCES

1 Saraste, M. (1999) Oxidative Phosphorylation at the fin de siècle. Science. **283**, 1488-1493

2 Pettigrew, G. W. and Moore, G. R. (1987) Cytochrome *c* - Biological Aspects. In Cytochrome *c* - Biological Aspects, Springer-Verlag, Berlin

3 Capitanio, N., Capitanio, G., Demarinis, D. A., De Nitto, E., Massari, S. and Papa, S. (1996) Factors Affecting the H+/e- Stoichiometry in Mitochondrial Cytochrome *c* Oxidase: Influence of the Rate of Electron Flow and Transmembrane Biochemistry. **35**, 10800-10806

4 Sakamoto, K., Kamiya, M., Imai, M., Shinzawa-Itoh, K., Uchida, T., Kawano, K., Yoshikawa, S. and Ishimori, K. (2011) NMR basis for interprotein electron transfer gating between cytochrome *c* and cytochrome *c* oxidase. Proc. Natl. Acad. Sci. USA. **108**, 12271-12276

5 Zhen, Y., Hoganson, C. W., Babcock, G. T. and Ferguson-Miller, S. (1999) Definition of the Interaction Domain for Cytochrome *c* on Cytochrome *c* Oxidase J. Biol. Chem. **274**, 38032 - 38041

6 Döpner, S., Hildebrandt, P., Rosell, F. I., Mauk, A. G., von Walter, M., Buse, G. and Soulimane, T. (1999) The structural and functional role of lysine residues in the binding domain of cytochrome *c* in the electron transfer to cytochrome *c* oxidase. Eur. J. Biochem. **261**, 379-391

7 Sato, W., Hitaoka, S., Inoue, K., Imai, M., Saio, T., Uchida, T., Shinzawa-Itoh, K., Yoshikawa, S., Yoshizawa, K. and Ishimori, K. (2016) Energetic Mechanism of Cytochrome *c*-Cytochrome *c* Oxidase Electron Transfer Complex Formation under Turnover Conditions Revealed by Mutational Effects and Docking Simulation. J. Biol. Chem. **291**, 15320-15331

8 Shimada, S., Shinzawa‐Itoh, K., Baba, J., Aoe, S., Shimada, A., Yamashita, E., Kang, J., Tateno, M., Yoshikawa, S. and Tsukihara, T. (2017) Complex structure of cytochrome *c*‐cytochrome *c* oxidase reveals a novel protein–protein interaction mode. EMBO J. **36**, 291-300

9 Furukawa, Y., Morishima, I. (2001) The Role of Water Molecules in the Association of Cytochrome P450cam with Putidaredoxin. J. Biol. Chem. **276**, 12983-12990

10 Chothia, C., Janin, J. (1975) Principles of protein-protein recognition. Nature. **256**, 705-708

11 Fiorucci, S. and Zacharias, M. (2010) Prediction of Protein-Protein Interaction Sites Using Electrostatic Desolvation Profiles. Biophys. J. **98**, 1921-1930

12 König, G., Bruckner, S. and Boresch, S. (2013) Absolute Hydration Free Energies of Blocked Amino Acids: Implications for Protein Solvation and Stability. Biophys. J. **104**, 453-462

13 Basdevant, N., Weinstein, H. and Ceruso, M. (2006) Thermodynamic Basis for Promiscuity and Selectivity in Protein-Protein Interactions: PDZ Domains, a Case Study. J. Am. Chem. Soc. **128**, 12766-12777

14 Jelesarov, I. and Bosshard, H. R. (1994) Thermodynamics of Ferredoxin Binding to Ferredoxin:$NADP^+$ Reductase and the Role of Water at the Complex Interface. Biochemistry. **33**, 13321-13328

15 Kimura, T., Sakamoto, K., Morishima, I. and Ishimori, K. (2006) Dehydration in the folding of reduced cytochrome *c* revealed by the electron-transfer-triggered folding under high pressure. J. Am. Chem. Soc. **128**, 670 -671

16 Rand, R. P., Fuller, N. L., Butko, P., Francis, G. and Nicholls, P. (1993) Measured change in protein solvation with substrate binding and turnover. Biochemistry. **32**, 5925-5929

17 Kornblatt, J. A., Kornblatt, M. J., Rajotte, I., Hoa, G. H. B., Kahn, P. C. (1998) Thermodynamic Volume Cycles for Electron Transfer in the Cytochrome *c* Oxidase and for the Binding of Cytochrome *c* to Cytochrome *c* Oxidase. Biophys. J. **75**, 435 - 444

18 Kornblatt, J. A., Kornblatt, M. J., Hoa, G. H. and Mauk, A. G. (1993) Responses of two protein-protein complexes to solvent stress: does water play a role at the interface? Biophys. J. **65**, 1059-1065

19 Lappalainen, P., Watmough, N. J., Greenwood, C. and Saraste, M. (1995) Electron transfer between cytochrome *c* and the isolated Cu_A domain: identification of substrate-binding residues in cytochrome *c* oxidase. Biochemistry. **34**, 5824-5830

20 Minnaert, K. (1961) The kinetics of cytochrome *c* oxidase. I. The system: cytochrome *c*-cytochrome oxidase-oxygen. Biochim. Biophys. Acta **50**, 23-34

21 Sakamoto, K., Kamiya, M., Uchida, T., Kawano, K. and Ishimori, K. (2010) Redox-controlled backbone dynamics of human cytochrome *c* revealed by ^{15}N NMR relaxation measurements. Biochem. Biophys. Res. Commun. **398**, 231-236

22 Jeng, W.-Y., Chen, C.-Y., Chang, H.-C. and Chuang, W.-J. (2002) Expression and Characterization of Recombinant Human Cytochrome *c* in *E. coli*. J. Bioenerg. Biomem. **34**, 423-431

23 Yoshikawa, S., Shinzawa-Itoh, K., Nakashima, R., Yaono, R., Yamashita, E., Inoue, N., Yao, M., Fei, M. J., Libeu, C. P., Mizushima, T., Yamaguchi, H., Tomizaki, T. and Tsukihara, T. (1998) Redox-coupled crystal structural changes in bovine heart cytochrome *c* oxidase. Science. **280**, 1723-1729

24 Weast, R. C. (1977) CRC Handbook of Chemistry and Physics. CRC Press, Inc. , Cleveland

25 Auton, M. and Bolen, D. W. (2005) Predicting the energetics of osmolyte-induced protein folding/unfolding. Proc. Natl. Acad. Sci. USA. **102**, 15065-15068

26 Bolen, D. W. and Baskakov, I. V. (2001) The osmophobic effect: natural selection of a thermodynamic force in protein folding1. J. Mol. Biol. **310**, 955-963

27 Schreiber, G., Haran, G. and Zhou, H. X. (2009) Fundamental Aspects of Protein−Protein Association Kinetics. Chem. Rev. **109**, 839-860

28 Wenner, J. R. and Bloomfield, V. A. (1999) Osmotic pressure effects on EcoRV cleavage and binding. J. Biomol. Struct. Dyn. . **17**, 461-471

29 Kuttner, Y. Y., Kozer, N., Segal, E., Schreiber, G. and Haran, G. (2005) Separating the Contribution of Translational and Rotational Diffusion to Protein Association. J. Am. Chem. Soc. **127**, 15138-15144

30 Michel, B. and Bosshard, H. R. (1989) Oxidation of cytochrome *c* by cytochrome *c* oxidase: spectroscopic binding studies and steady-state kinetics support a conformational transition mechanism. Biochemistry. **28**, 244-252

31 Ferguson-Miller, S., Brautigan, D. L. and Margoliash, E. (1978) Definition of cytochrome *c* binding domains by chemical modification. III. Kinetics of reaction of carboxydinitrophenyl cytochromes *c* with cytochrome *c* oxidase. J. Biol. Chem. **253**, 149-159

32 Hou, T., Wang, J., Li, Y. and Wang, W. (2011) Assessing the Performance of the MM/PBSA and MM/GBSA Methods. 1. The Accuracy of Binding Free Energy Calculations Based on Molecular Dynamics Simulations. J. Chem. Inf. Model. **51**, 69-82

33 Hitaoka, S. and Chuman, H. (2013) Revisiting the Hansch–Fujita approach and development of a fundamental QSAR. J. Pestic. Sci. **38**, 60-67

34 Speck, S. H., Dye, D. and Margoliash, E. (1984) Single catalytic site model for the oxidation of ferrocytochrome *c* by mitochondrial cytochrome *c* oxidase. Proc. Natl. Acad. Sci. USA. **81**, 347-351

35 Timasheff, S. N. (1993) The control of protein stability and association by weak interactions with water: how do solvents affect these processes? Annu. Rev. Biophys. Biomol. Struct. . **22**, 67-97

36 Davis-Searles, P. R., Saunders, A. J., Erie, D. A., Winzor, D. J. and Pielak, G. J. (2001) Interpreting the Effects of Small Uncharged Solutions on Protein-folding Equilibria. Annu. Rev. Biophys. Biomol. Struct. . **30**, 271-306

37 Scharlau, M., Geren, L., Zhen, E. Y., Ma, L., Rajagukguk, R., Ferguson-Miller, S., Durham, B. and Millett, F. (2019) Definition of the Interaction Domain and Electron Transfer Route between Cytochrome *c* and Cytochrome Oxidase. Biochemistry. **58**, 4125-4135

38 Gekko, K. and Noguchi, H. (1979) Compressibility of globular proteins in water at 25.degree.C. J. Phys. Chem. **83**, 2706-2714

39 Rossky, P. J. and Karplus, M. (1979) Solvation. A molecular dynamics study of a dipeptide in water. J. Am. Chem. Soc. **101**, 1913-1937

40 Suzuki, M., Shigematsu, J., Fukunishi, Y., Harada, Y., Yanagida, T. and Kodama, T. (1997) Coupling of protein surface hydrophobicity change to ATP hydrolysis by myosin motor domain. Biophys. J. **72**, 18-23

41 Rajagopal, Badri S., Edzuma, Ann N., Hough, Michael A., Blundell, Katie L. I. M., Kagan, Valerian E., Kapralov, Alexandr A., Fraser, Lewis A., Butt, Julea N., Silkstone, Gary G., Wilson, Michael T., Svistunenko, Dimitri A. and Worrall, Jonathan A. R. (2013) The hydrogen-peroxide-induced radical behaviour in human cytochrome *c*–phospholipid complexes: implications for the enhanced pro-apoptotic activity of the G41S mutant. Biochem. J. **456**, 441-452

42 Shinzawa-Itoh, K., Aoyama, H., Muramoto, K., Terada, H., Kurauchi, T., Tadehara, Y., Yamasaki, A., Sugimura, T., Kurono, S., Tsujimoto, K., Mizushima, T., Yamashita, E., Tsukihara, T. and Yoshikawa, S. (2007) Structures and physiological roles of 13 integral lipids of bovine heart cytochrome c oxidase. EMBO J. **26**, 1713-1725

43 Palese, L. L. (2020) Oxygen-oxygen distances in protein-bound crystallographic water suggest the presence of protonated clusters. Biochim. Biophys. Acta. **1864**, 129480

44 Suzuki, M., Shigematsu, J., Fukunishi, Y. and Kodama, T. (1997) Hydrophobic Hydration Analysis on Amino Acid Solutions by the Microwave Dielectric Method. J. Phys. Chem. B. **101**, 3839-3845

45 Yonetani, T. and Ray, G. S. (1965) Studies on Cytochrome Oxidase: VI. KINETICS OF THE AEROBIC OXIDATION OF FERROCYTOCHROME *c* BY CYTOCHROME OXIDASE. J. Biol. Chem. **240**, 3392-3398

46 Yoshikawa, S. and Shimada, A. (2015) Reaction Mechanism of Cytochrome *c* Oxidase. Chem. Rev. **115**, 1936-1989

47 Bloch, D., Belevich, I., Jasaitis, A., Ribacka, C., Puustinen, A., Verkhovsky, M. I. and Wikström, M. (2004) The catalytic cycle of cytochrome *c* oxidase is not the sum of its two halves. Proc. Natl. Acad. Sci. USA. **101**, 529-533

48 Makhatadze, G. I. and Privalov, P. L. (1995) Energetics of Protein Structure. Advan. Protein Chem. **47**, 307-425

49 Luque, I. and Freire, E. (1998) Structure-based prediction of binding affinities and molecular design of peptide ligands. Methods. Enzymol. **295**, 100-127

50 de la Lande, A., Babcock, N. S., Řezáč, J., Sanders, B. C. and Salahub, D. R. (2010) Surface residues dynamically organize water bridges to enhance electron transfer between proteins. Proc. Natl. Acad. Sci. USA. **107**, 11799-11804

51 Nojiri, M., Koteishi, H., Nakagami, T., Kobayashi, K., Inoue, T., Yamaguchi, K. and Suzuki, S. (2009) Structural basis of inter-protein electron transfer for nitrite reduction in denitrification. Nature. **462**, 117-120

52 Tipmanee, V., Oberhofer, H., Park, M., Kim, K. S. and Blumberger, J. (2010) Prediction of Reorganization Free Energies for Biological Electron Transfer: A Comparative Study of Ru-Modified Cytochromes and a 4-Helix Bundle Protein. J. Am. Chem. Soc. **132**, 17032-17040

53 Williamson, D. A. and Bowler, B. E. (1998) Electron Transfer through the Hydrogen-Bonded Interface of a β-Turn-Forming Depsipeptide. J. Am. Chem. Soc. **120**, 10902-10911

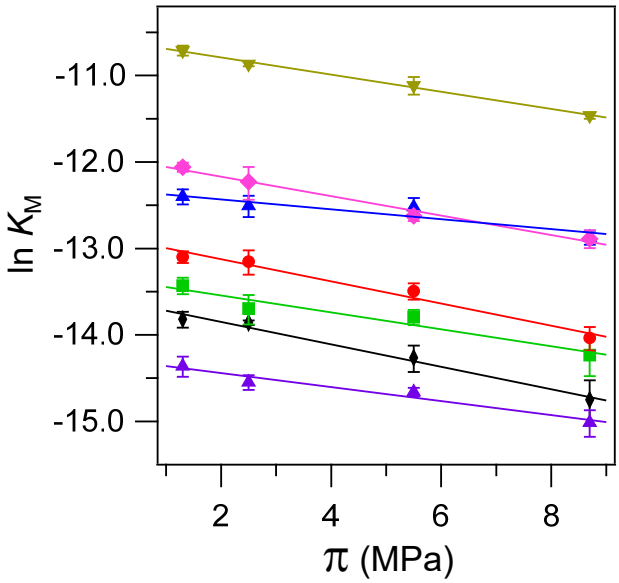

Figure 1. Dependence of the Michaelis constants (K_M) on osmotic pressure for formation of Cyt *c* – C*c*O complex. Each osmolyte was added to obtain a viscosity of 1.6 mPa·s (sucrose: 1.3 MPa, D-glucose: 2.5 MPa, glycerol: 5.5 MPa, ethylene glycol: 8.7 MPa). Error bars represent ln (K_M ± S.D.). wild-type (WT), red; I9A, black; I11A, green; K13A, yellowish brown; K79A, pink; I81A, blue; I81S, purple.

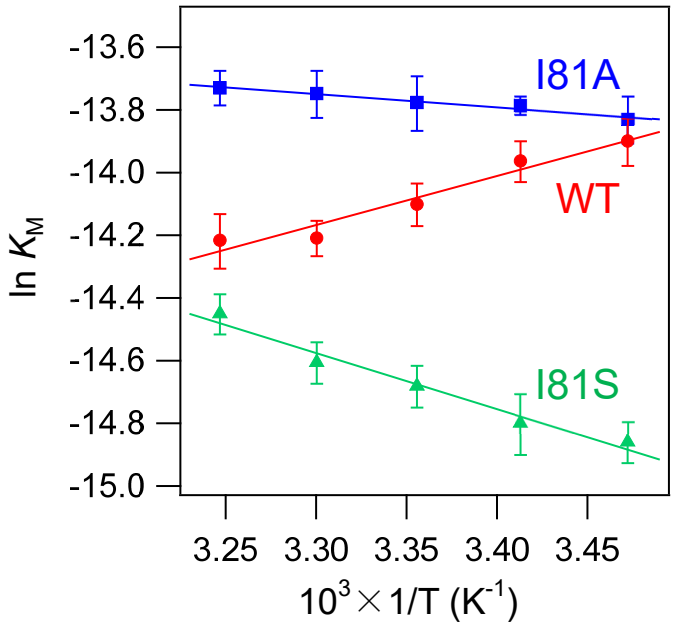

Figure 2. Temperature dependence of the Michaelis constant (K_M) for Cyt *c* – C*c*O complex formation. Experimental conditions: 50 mM sodium phosphate buffer at pH 6.8 containing 0.1% n-decyl-β-D-maltoside. Error bars represent ln ($K_M \pm$ S.D.). wild-type (closed circle); I81A (closed square), I81S (closed triangle)

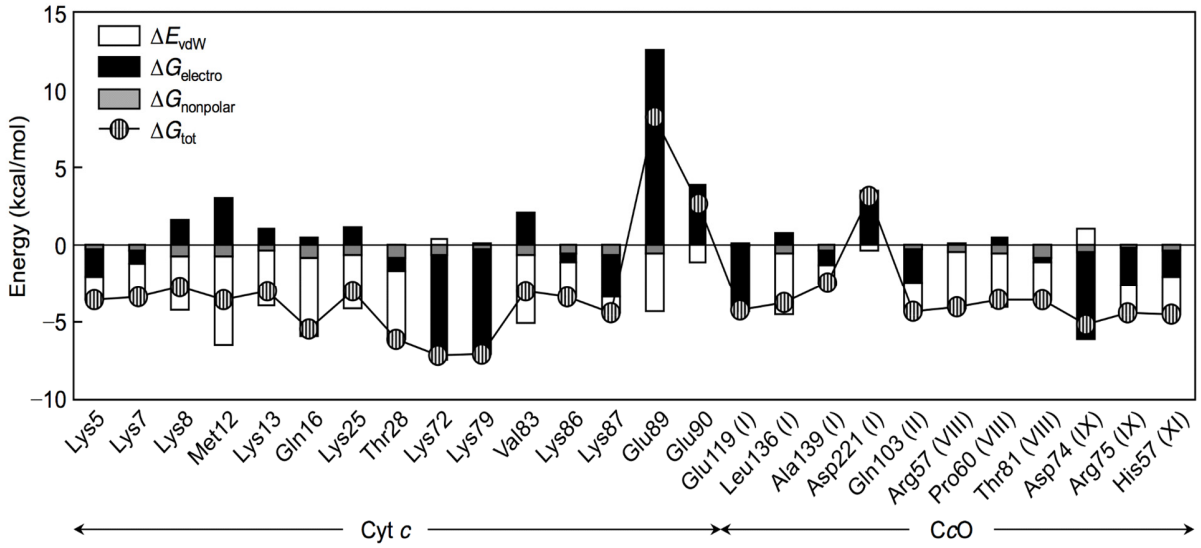

Figure 3. Free energy decomposition of ΔG_{tot} (= ΔG_{bind} + ΔG_{sol}) on a per residue basis into the contributions from ΔE_{vdW}, $\Delta G_{electro}$, and $\Delta G_{nonpolar}$ in I81S Cyt *c* mutant. Residues with a $|\Delta G_{tot}|$ value rounded off to the nearest integer ≥ 3.0 kcal mol^{-1} are shown.

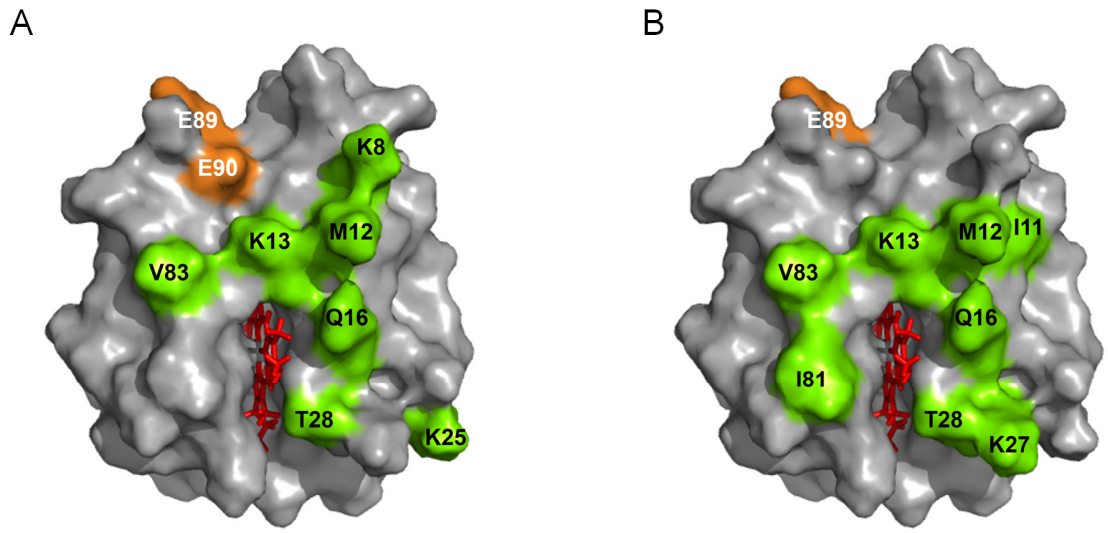

Figure 4. Amino acid residues of Cyt *c* forming hydrophobic interaction with C*c*O ($|\Delta E_{vdW} + \Delta G_{nonpolar}| \geq 2.5$ kcal mol^{-1}) based on the energy analysis shown in Figure 3. The total interaction energy of Glu89 and Glu90 in the I81 mutant and that of Glu89 in wild-type Cyt *c* are positive due to the large electrostatic repulsion energy. wild-type (A) ; I81S (B)

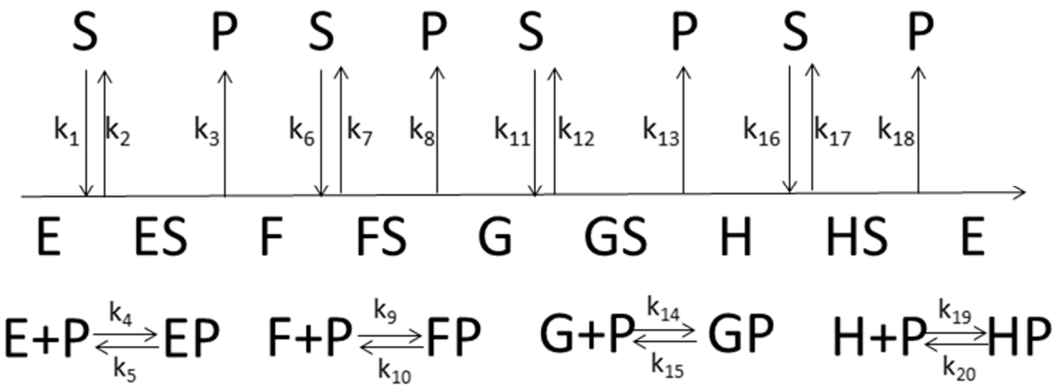

Figure 5. Schematic representation of four-electron reduction in C*c*O by Cyt *c*. The four intermediate C*c*O species are designated as E, F, G and H. S and P represent Cyt c^{2+} and Cyt c^{3+}, respectively.

Table 1. Osmotic pressure dependence of the dissociation constants for formation of Cyt *c* – C*c*O complex.

Osmotic pressure (π) (MPa)	K_M (μM)	Osmolyte and concentration	Water activity
1.3	2.05 ± 0.14	15.2% Sucrose	0.991
2.5	1.94 ± 0.27	15.6% D-Glucose	0.982
5.5	1.38 ± 0.13	17.5% Glycerol	0.960
8.7	0.80 ± 0.11	18.6% Ethylene glycol	0.938

Table 2. Volume changes and numbers of the dehydrated water molecule associated with formation of the Cyt *c* – C*c*O complex

Cyt *c*	ΔV (mL mol^{-1})	Number of dehydrated water molecule
Wild-type	314 ± 50	17 ± 3
I9A	317 ± 48	18 ± 3
I11A	246 ± 72	14 ± 4
I81A	139 ± 38	8 ± 2
I81S	197 ± 38	11 ± 3
K13A	241 ± 20	13 ± 1
K79A	278 ± 44	15 ± 2

Table 3. Thermodynamic parameters for formation of the ES complex between Cyt *c* and C*c*O at 293K.

Cyt *c*	ΔH (kJmol^{-1})	ΔS (JK^{-1}mol^{-1})
Wild-type	13.0 ± 1.6	161 ± 6
I81A	- 3.53 ± 3.01	103 ± 10
I81S	- 14.9 ± 1.4	72 ± 5

Supporting Material for

Osmotic pressure effects identify dehydration upon cytochrome *c* - cytochrome *c* oxidase complex formation contributing to a specific electron pathway formation

Wataru Sato[1], *Seiji Hitaoka*[2], *Takeshi Uchida*[1,3], *Kyoko Shinzawa-Itoh*[4], *Kazunari Yoshizawa*[2], *Shinya Yoshikawa*[4], *and Koichiro Ishimori*[1,3,*]

[1]Graduate School of Chemical Sciences and Engineering, Hokkaido University, Sapporo 060-8628, Japan,

[2]Institute for Materials Chemistry and Engineering, Kyushu University, Fukuoka 819-0315, Japan,

[3]Department of Chemistry, Faculty of Science, Hokkaido University, Sapporo 060-0810, Japan,

[4]Picobiology Institute, Graduate School of Life Science, University of Hyogo, Ako-gun, Hyogo 678-1297, Japan.

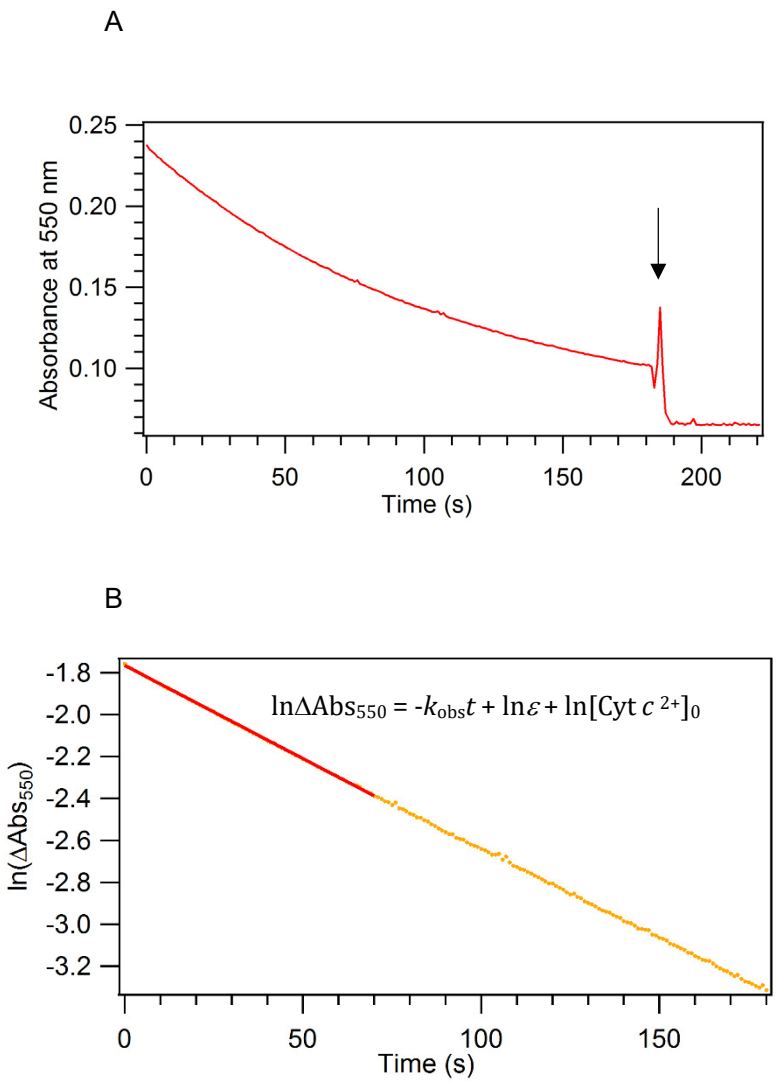

Figure S1. Absorbance change at 550 nm after the addition of C*c*O. (A) A small amount of potassium ferricyanide (III) was added to the reaction mixture (downward allow) to determine the end point of the electron transfer reaction. The measurements were carried out in the presence of 1 nM C*c*O dissolved in 50 mM sodium phosphate buffer at pH 6.8, 293 K, containing 0.1 % *n*-decyl β-D-maltoside. (B) Log-plots of the absorbance change at 550 nm against time from 0 s - 70 s. The apparent rate constants, k_{obs}, at the various concentrations of Cyt *c* were determined by using the following equation: $\ln\Delta Abs_{550} = -k_{obs}\, t + \ln\varepsilon + \ln[\text{Cyt } c^{2+}]_0$

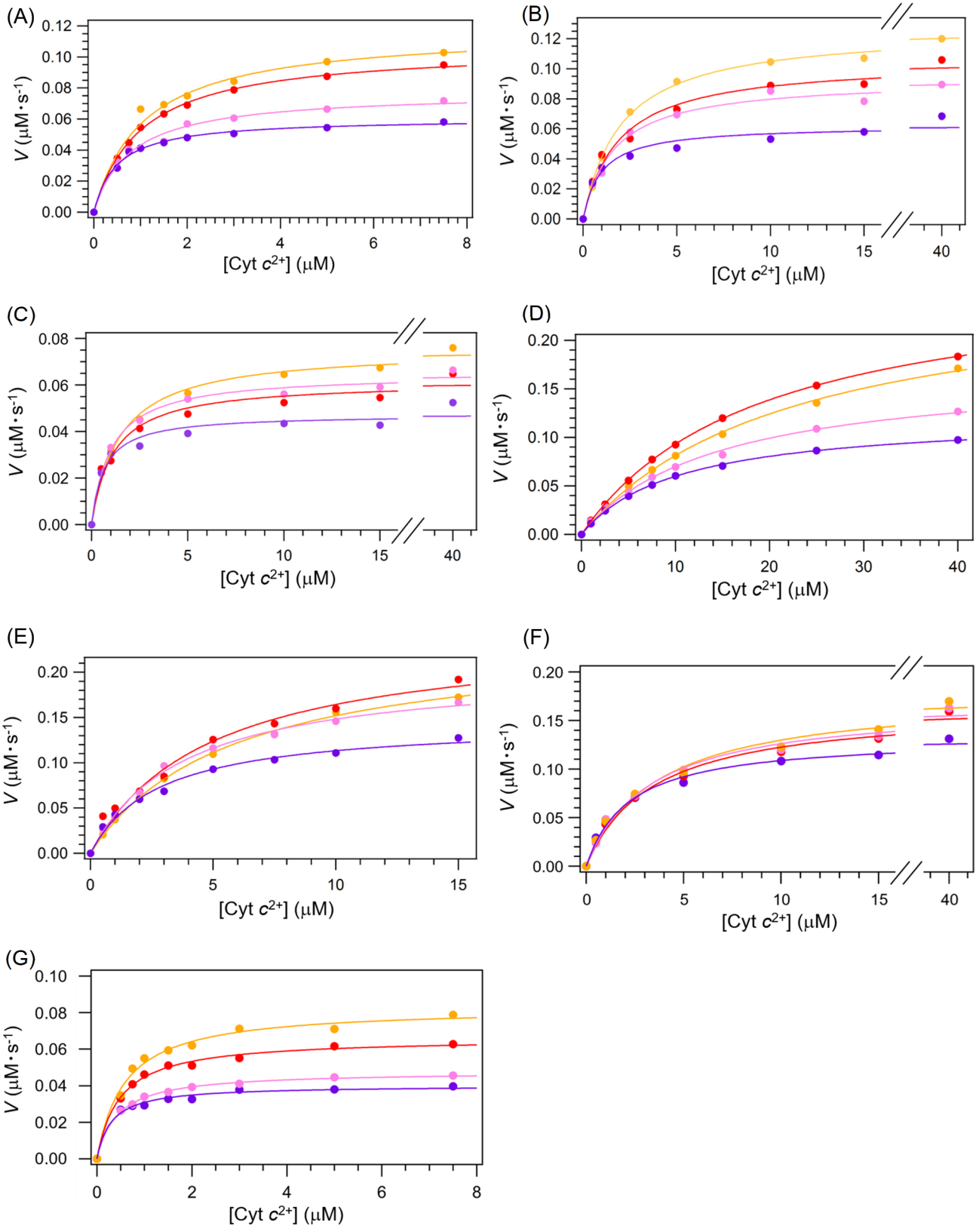

Figure S2. The dependence of the initial rate constants on the concentrations of wild-type and mutant Cyt *c* in the presence of various kinds of osmolytes. A, wild-type; B, I9A; C, I11A; D, K13A; E, K79A, F, I81A; G, I81S. Sucrose, orange; D-Glucose, red; Glycerol, pink, and Ethylene glycol, purple. The solid curves are best fits to the Michaelis-Menten equation using least-square analysis.

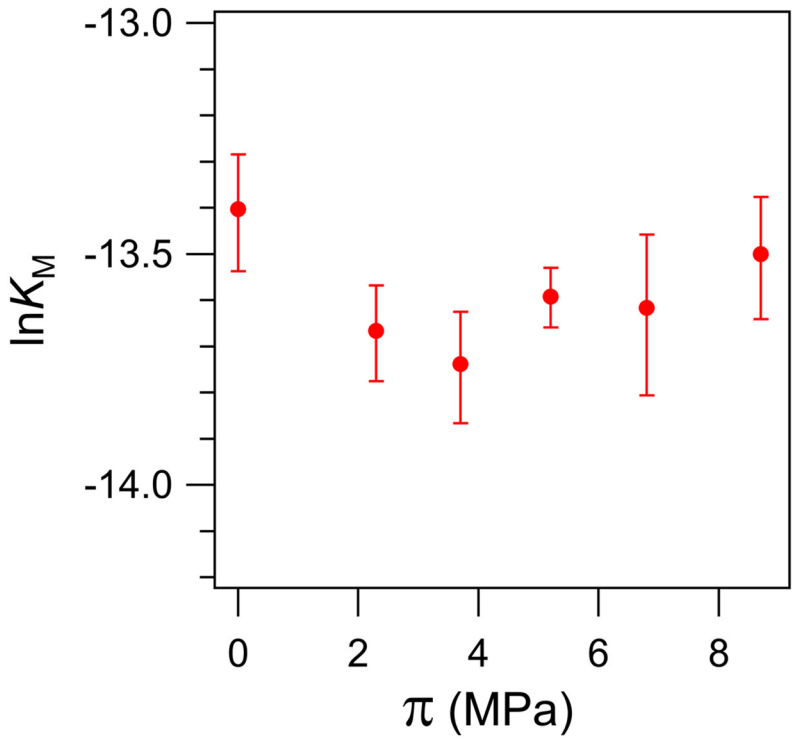

Figure S3. Dependence of K_M for the electron transfer reaction from Cyt *c* to C*c*O on osmotic pressure under various concentrations of glycerol. K_M value was decreased with increasing the osmotic pressure up to 3.7 MPa. In high osmotic pressure region ($\pi > 5$ MPa), however, K_M was increased with the addition of glycerol due to its increased viscosity from 1.002 mPa·s (0% glycerol; $\pi = 0$ MPa) to 1.998 mPa·s (24% glycerol; $\pi = 8.7$ MPa) at 293 K[1]. Error bars represent ln (K_M ±S.D.).

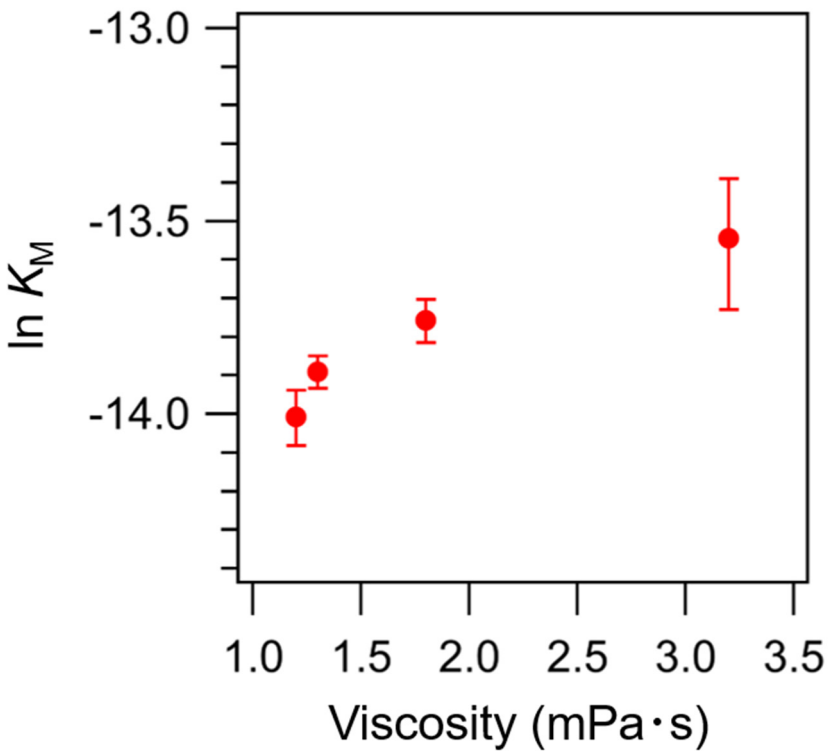

Figure S4. Dependence of the Michaelis constants (K_M) on solution viscosity for formation of Cyt *c*-C*c*O complex. Each osmolyte was added to obtain an osmotic pressure of 3.0 MPa (7.14% ethylene glycol: 1.19 mPa·s, 10.3% glycerol: 1.27 mPa·s, 18.4% D-glucose: 1.77 mPa·s, 29.9% sucrose: 3.18 mPa·s). Error bars represent ln (K_M ±S.D.).

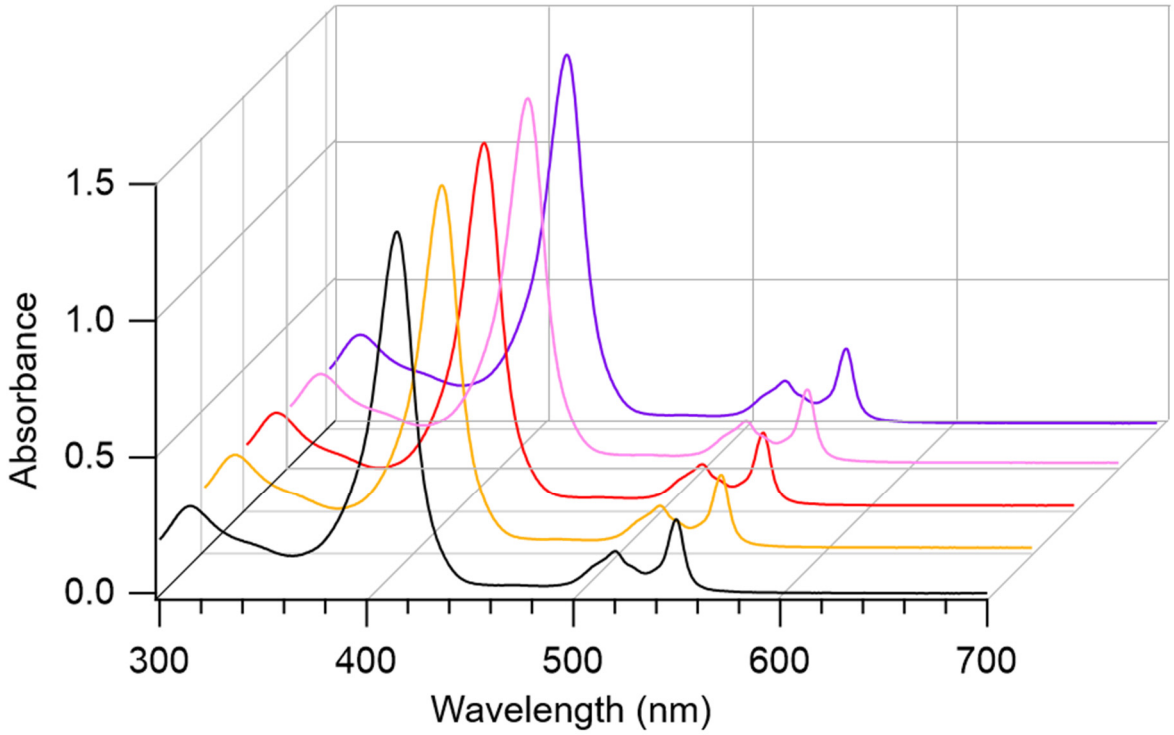

Figure S5. Absorption spectra of Cyt *c* in the presence of various kinds of osmolytes. 0% osmolyte (NaPi buffer), black; 15.2% Sucrose, orange; 15.6% D-Glucose, red; 17.5% Glycerol, pink, and 18.6% Ethylene glycol, purple.

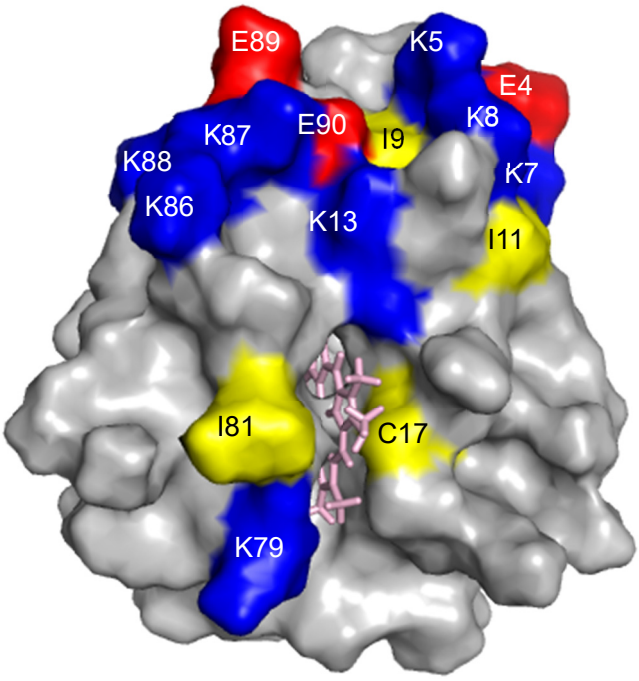

Figure S6. Interaction Site of Cyt *c* for C*c*O[2]. Positively charged residue, blue; Negatively charged residues, red; Hydrophobic residue, yellow.

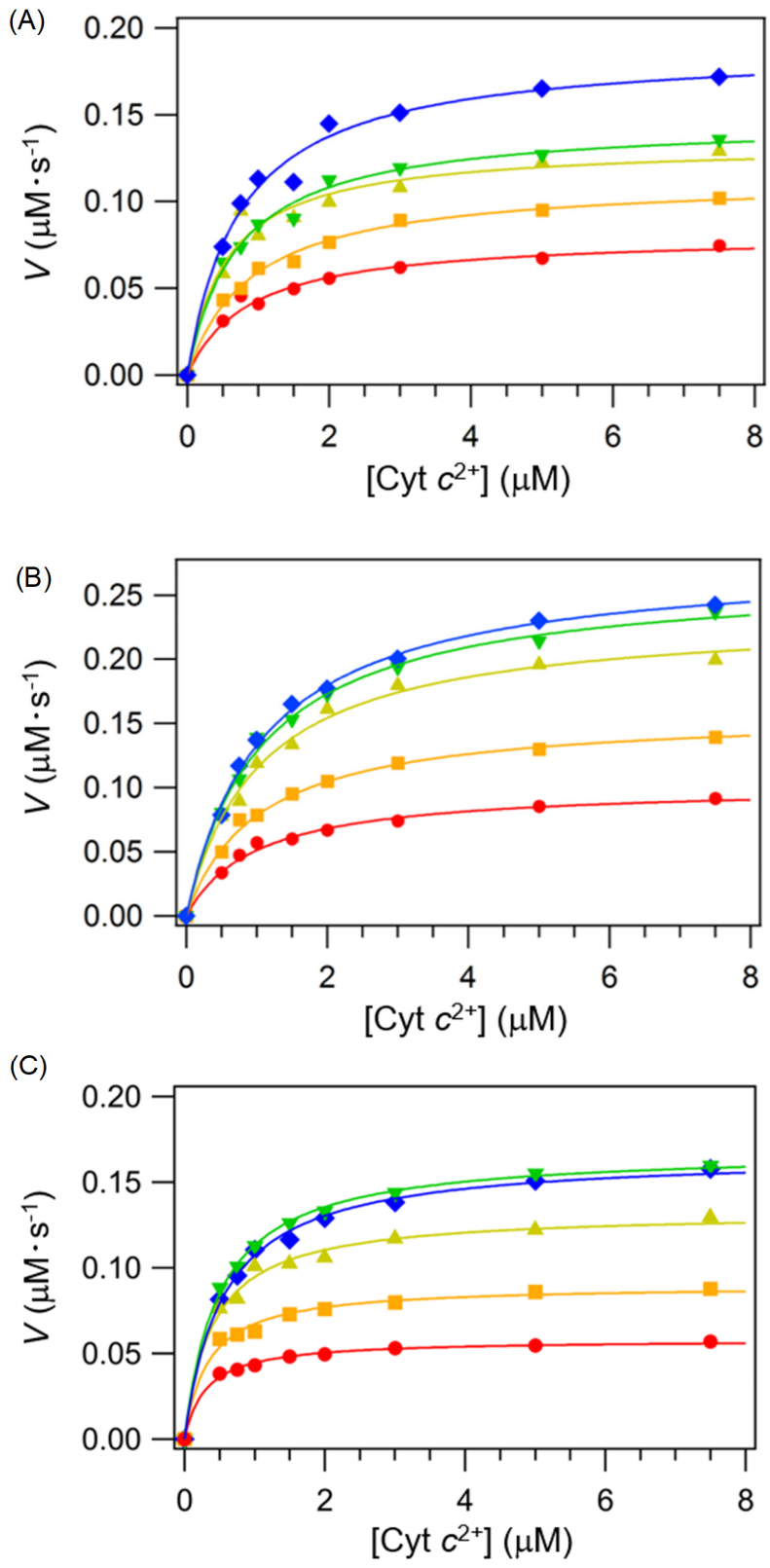

Figure S7. The dependence of the initial rate constants on the concentrations of wild-type and mutant Cyt *c* at various temperatures. A, wild-type; B, I81A; C, I81S. The measurement temperatures are 288K (●), 293K (■), 298K (▲), 303K (▼), and 308K (◆). The solid curves are best fits to the Michaelis-Menten equation using least-square analysis.

A

B

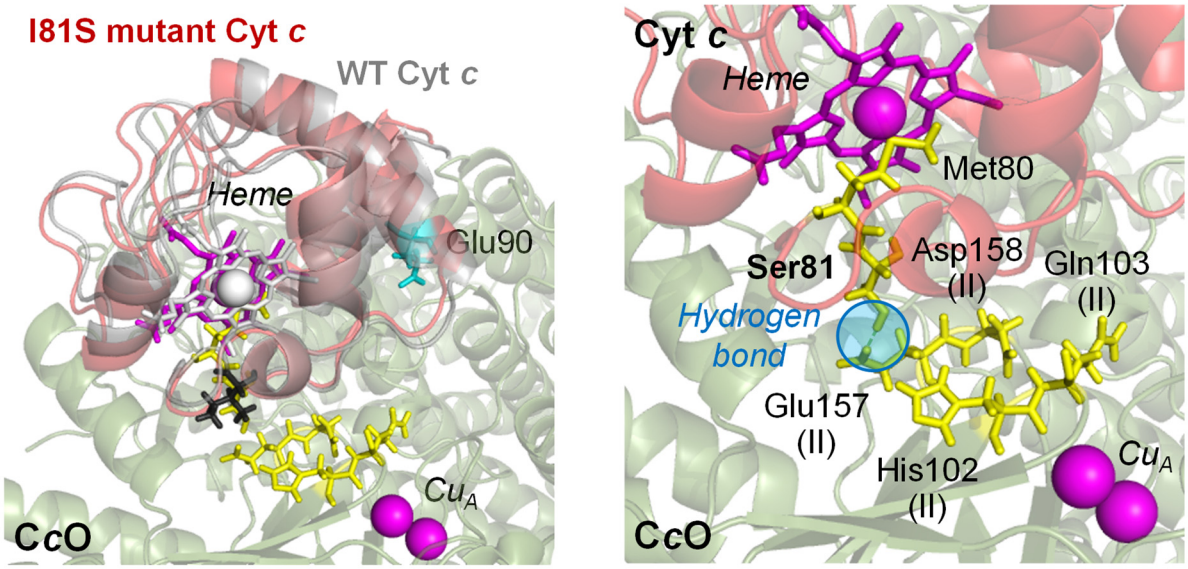

Figure S8. The binding orientation of wild type and I81S Cyt *c* on CcO and enlarged view of the residues at the region of interface between I81S Cyt *c* and C*c*O. (A) The predicted complex structure between I81S Cyt *c* and C*c*O is overlapped with the predicted complex structure of wild type Cyt *c* and C*c*O. (B) A new hydrogen bond is formed between Ser81 in I81S Cyt *c* and Glu157 in subunit II of C*c*O.

Table S1. Primer sequences for Cyt *c* mutants

Cyt *c*	Mutation site	Primer sequence (Upper: Sense, Lower: Anti-sense)[a]
I9A	Ile9 → Ala	5′-AAG-AAG-GCG-TTT-ATT-ATG-AAG-TGT-TCC-3′ 3′-CAA-CTC-TTT-CCG-TTC-TTC-CGC-AAA-TAA-5′
I11A	Ile11 → Ala	5′-ATT-TTT-GCG-ATG-AAG-TGT-TCC-CAG-TGC-3′ 3′-TTT-CCG-TTC-TTC-TAA-AAA-CGC-TAC-TTC-3′
L13A	Lys13 → Ala	5′-ATT-ATG-GCC-TGT-TCC-CAG-TGC-CAC-ACT-3′ 3′-TTC-TTC-TAA-AAA-TAA-TAC-CGG-ACA-AGG-5′
L79A	Lys79 → Ala	5′-GGA-ACA-GCC-ATG-ATC-TTT-GTC-GGC-ATT-3′ 3′-TTC-ATG-TAG-GGA-CCT-TGT-CGG-TAC-TAG-5′
I81A	Ile81 → Ala	5′-AAA-ATG-GCG-TTT-GTC-GGC-ATT-AAG-AAG-3′ 3′-TAG-GGA-CCT-TGT-TTT-TAC-CGC-AAA-CAG-5′
I81S	Ile81 → Ser	5′-AAA-ATG-ACG-TTT-GTC-GGC-ATT-AAG-AAG-3′ 3′-TAG-GGA-CCT-TGT-TTT-TAC-TGC-AAA-CAG-5′

[a]Underlined codons denote the mutation sites.

Table S2. Composition of the reaction medium (50 mM NaPi buffer, pH 6.8, 0.1% DM)

Osmolyte and concentration	Solvent activity	pK_a[a]	[$H_2PO_4^-$] (mM)	[HPO_4^{2-}] (mM)	Ionic strength (mM)[b]
0% osmolyte	0.999	7.21[1]	36.0	14.0	80.2
15.2% sucrose	0.991	7.26	37.0	13.0	78.7
15.6% D-glucose	0.982	7.26	37.1	12.9	78.5
17.5% glycerol	0.960	7.28	37.6	12.4	77.8
18.6% ethylene glycol	0.938	7.29	37.8	12.2	77.5

[a] Acid dissociation constant for $H_2PO_4^- \rightleftharpoons H^+ + HPO_4^{2-}$.

[b] To adjust the pH of the NaPi buffer, 0.0183 M NaOH was added.

Table S3. Hydrated water molecules around some residues in the interaction site of Cyt *c* for C*c*O

Amino acid residues	Fraction of ASA[a] (%)	${}^{hydr}N$[b]
Ile9	15	~1
Ile11	42	~4
Lys13	30	~3
Lys79	89	~9
Ile81	85	~7

[a]Accessible surface area to solvent. These values were calculated by using the web server "VADAR"[3]. We used structural data from Protein Data Bank (PDB) (PDB code; 1J3S).

[b]The number of hydrated water molecules. This number was calculated by the following equation:

$${}^{hydr}N = \text{ASA (\%)} / 100 \times {}^{hydr}N \text{ (amino acid residue)}$$

where ASA is the accessible surface area to solvent and ${}^{hydr}N$ (amino acid residue) is the number of the hydrated water molecules of the isolated amino acid residue. We use 8.60 and 1.75 as ${}^{hydr}N$ (amino acid residue) for Ile and Ala residues, respectively[4].

Table S4. Michaelis constants of wild type and mutant Cyt *c* for C*c*O under various osmotic pressure

Osmolyte	Osmotic pressure (MPa)	K_M (μM)						
		WT	I9A	I11A	K13A	K79A	I81A	I81S
sucrose	1.3	2.05 ± 0.14	0.996 ± 0.091	1.47 ± 0.14	22.3 ± 1.3	5.79 ± 0.30	4.12 ± 0.36	0.579 ± 0.067
D-glucose	2.5	1.94 ± 0.27	0.956 ± 0.026	1.13 ± 0.19	19.1 ± 0.5	4.98 ± 0.92	3.70 ± 0.45	0.481 ± 0.041
glycerol	5.5	1.38 ± 0.13	0.639 ± 0.097	1.02 ± 0.09	14.9 ± 1.5	3.29 ± 0.19	3.65 ± 0.41	0.430 ± 0.021
ethylene glycol	8.7	0.804 ± 0.109	0.393 ± 0.099	0.657 ± 0.141	10.5 ± 0.4	2.53 ± 0.26	2.57 ± 0.21	0.302 ± 0.046

Table S5. Turnover constants of wild type and mutant Cyt *c* for C*c*O under various osmotic pressure

Osmolyte	Osmotic pressure (MPa)	k_{cat} (s^{-1})						
		WT	I9A	I11A	K13A	K79A	I81A	I81S
sucrose	1.3	126 ± 2	125 ± 4	78.4 ± 1.5	262 ± 8	240 ± 6	180 ± 4	83.2 ± 2.5
D-glucose	2.5	105 ± 3	115 ± 1	61.4 ± 2.1	271 ± 4	246 ± 9	164 ± 5	66.0 ± 1.3
glycerol	5.5	99.0 ± 2.0	75.3 ± 2.9	64.8 ± 1.1	174 ± 9	205 ± 7	167 ± 5	47.8 ± 0.5
ethylene glycol	8.7	58.5 ± 1.6	44.8 ± 1.2	47.3 ± 1.7	123 ± 2	145 ± 7	133 ± 3	40.2 ± 0.9

Table S6. Michaelis constants of wild type and mutant Cyt *c* for C*c*O under various temperature

Temperature (K)	K_M (μM)		
	WT	I81A	I81S
288	0.920 ± 0.070	0.986 ± 0.074	0.352 ± 0.023
293	0.863 ± 0.056	1.03 ± 0.03	0.374 ± 0.036
298	0.752 ± 0.051	1.04 ± 0.09	0.421 ± 0.028
303	0.675 ± 0.038	1.07 ± 0.08	0.454 ± 0.030
308	0.670 ± 0.058	1.09 ± 0.06	0.530 ± 0.034

Table S7. Turnover constants of wild type and mutant Cyt *c* for C*c*O under various temperature

Temperature (K)	k_{cat} (s^{-1})		
	WT	I81A	I81S
288	86.8 ± 1.8	102 ± 2	57.9 ± 0.7
293	110 ± 3	158 ± 1	96.0 ± 1.7
298	139 ± 2	234 ± 7	133 ± 2
303	147 ± 2	266 ± 7	167 ± 2
308	165 ± 4	278 ± 5	165 ± 3

References

[1] R.C. Weast, CRC Handbook of Chemistry and Physics CRC Press, Inc , Cleveland, (1977).

[2] K. Sakamoto, M. Kamiya, M. Imai, K. Shinzawa-Itoh, T. Uchida, K. Kawano, S. Yoshikawa, K. Ishimori, NMR basis for interprotein electron transfer gating between cytochrome *c* and cytochrome *c* oxidase, Proc. Natl. Acad. Sci. U. S. A., 108 (2011) 12271–12276.

[3] L. Willard, A. Ranjan, H. Zhang, H. Monzavi, R.F. Boyko, B.D. Sykes, D.S. Wishart, VADAR: A web server for quantitative evaluation of protein structure quality, Nucleic Acids Res., 31 (2003) 3316–3319.

[4] M. Suzuki, J. Shigematsu, Y. Fukunishi, T. Kodama, Hydrophobic hydration analysis on amino acid solutions by the microwave dielectric method, J. Phys. Chem. B, 101 (1997) 3839–3845.